

MECHANICAL AND IN VITRO CORROSION BEHAVIOUR OF Fe-CONTAINING TiNb(Zr-Fe)Ta ALLOYS

S. GONZÁLEZ^{a*}, E. PELLICER^a, E. ROSSINYOL^b, S. SURINACH^a, M.D. BARÓ^a, J. SORT^c

^a*Departament de Física, Universitat Autònoma de Barcelona, 08193 Bellaterra, Spain*

^b*Servei de Microscòpia, Universitat Autònoma de Barcelona, 08193 Bellaterra, Spain*

^c*Institució Catalana de Recerca i Estudis Avançats and Departament de Física, Universitat Autònoma de Barcelona, 08193 Bellaterra, Spain*

The mechanical behaviour and corrosion resistance, in simulated body fluid, of novel Ti-45Nb-(7-x)Zr-12.5Ta-xFe (x = 0, 3 and 7 wt. %) alloys have been investigated. Partial substitution of Zr by Fe, a cheaper β -stabilizing element, allows decreasing the Young's modulus and slightly improving the wear resistance. Moreover, moderate additions of Fe shift the corrosion potential towards more positive values, thus making these materials suitable for biomedical applications.

(Received February 17, 2012; Accepted May 7, 2012)

Keywords: Metals and alloys; Rapid solidification; Corrosion

1. Introduction

Titanium alloys are potential candidates to be used as metallic biomaterials due to their biocompatibility, low Young's modulus and good corrosion resistance [1]. One of the most widely used alloys for orthopaedic implants is Ti-6Al-4V [2], although it suffers from some drawbacks: adverse health effects arise from release of Al and V ions into the human body [3] and this alloy exhibits relatively high Young's modulus as compared to that of bone [1]. To overcome these limitations, non-toxic β -stabilizing alloys have been developed in order to improve both biochemical and biomechanical compatibility. By favouring the formation of β phase, the Young's modulus of the alloy can be decreased to facilitate the load transfer from the implant to the bone, avoiding bone resorption and final loosening of the implant. Alloys corresponding to the Ti-Nb-Zr-Ta system (TNZT) are particularly interesting since not only the constituting elements are non-toxic but also their Young's modulus is the lowest amongst Ti alloys [4]. Despite the potential interest of these alloys as biomaterials their corrosion behaviour has not been extensively studied [5].

The aim of the present work is to investigate the effect of partial and total substitution of Zr by Fe, a cheaper element which stabilizes the β -phase even more than Zr, on the mechanical and corrosion behaviour of the Ti-45Nb-(7-x)Zr-12.5Ta-xFe (x = 0, 3 and 7 wt. %) alloy.

2. Experimental procedure

Master alloys with composition Ti-45Nb-(7-x)Zr-12.5Ta-xFe (x = 0, 3 and 7 wt. %) were prepared by arc melting from a mixture of pure elements (> 99.9 at. %) in a Ti-gettered high purity

*Corresponding author: Sergio.Gonzalez@uab.es

argon atmosphere. The master alloys were then remelted at least three times to get chemically homogeneous ingots. Rod samples of 2 mm in diameter were obtained from the melt by injecting the master alloy into a copper mould in an inert gas atmosphere. The structure of the as-cast rods was studied by X-ray diffraction (XRD) (Phillips X'Pert) with monochromatic Cu-K α radiation. The microstructure was observed with a scanning electron microscope (SEM) (MERLIN) equipped with energy dispersive X-ray (EDX) analysis. Further microstructural characterization was performed by means of transmission electron microscopy (JEOL JEM-2011), along with EDX and selected area electron diffraction (SAED) studies, for compositional and crystallographic analyses, respectively.

The elastic properties were evaluated at room temperature by means of ultrasonic measurements (pulse-echo overlap technique), using an ultrasonic pulser-receiver model 5072PR and an oscilloscope model TDS 2022B Textronix, together with density assessment (Archimedes' method). Nanoindentation experiments were carried out in a UMIS equipment, at room temperature, on the disks' cross sections at approximately half the radius distance from the rod centre, using a Berkovich-type tip in the load control mode. Prior to nanoindentation, the specimens were polished until the surface had a mirror-like appearance. The indentation function consisted of a loading segment of 120 s to a maximum load of 500 mN, followed by a load holding segment of 30 s and an unloading segment of 150 s. The thermal drift was kept below 0.05 nm/s. The results correspond to the average of a total of 50 indentations for each sample. The hardness (H) and reduced elastic modulus (E_r) values were derived from these load-displacement curves using the method of Oliver and Pharr [6]. The corrosion behaviour of the samples was studied by electrochemical techniques in a simulated body fluid (Hank's solution) at 37°C. The electrochemical experiments were performed in a thermostated, one-compartment three-electrode cell. A double junction Ag|AgCl reference electrode was used with 3 M KCl inner solution and 1 M NaCl outer solution. A Pt sheet acted as a counter electrode. Initially, the specimens were immersed in the Hank's solution to determine the open circuit potential (OCP). Immediately after the potential became stable, the potential was swept anodically at a rate of 0.1 mV s $^{-1}$, beginning about 300 mV below the OCP. The corrosion current density (j_{corr}) values were determined by extrapolation of the anodic and cathodic Tafel slopes to the corrosion potential (E_{corr}).

3. Results and discussion

Fig. 1(a-c) show the SEM images (backscattered electrons) of the as-cast Ti-45Nb-(7-x)Zr-12.5Ta-xFe ($x = 0, 3$ and 7 wt. %) respectively. A magnified SEM image at about half the radius of each rod is shown in the upper insets of Fig. 1. The microstructure consists of a finely distributed dendritic phase of 20 μm in size together with a few larger regions of about 200 μm (larger red arrow), both rich in Nb and Ta (i.e., brighter phase), embedded in a matrix of darker tonality which is rich in Ti, Zr and Fe (according to the EDX analyses).

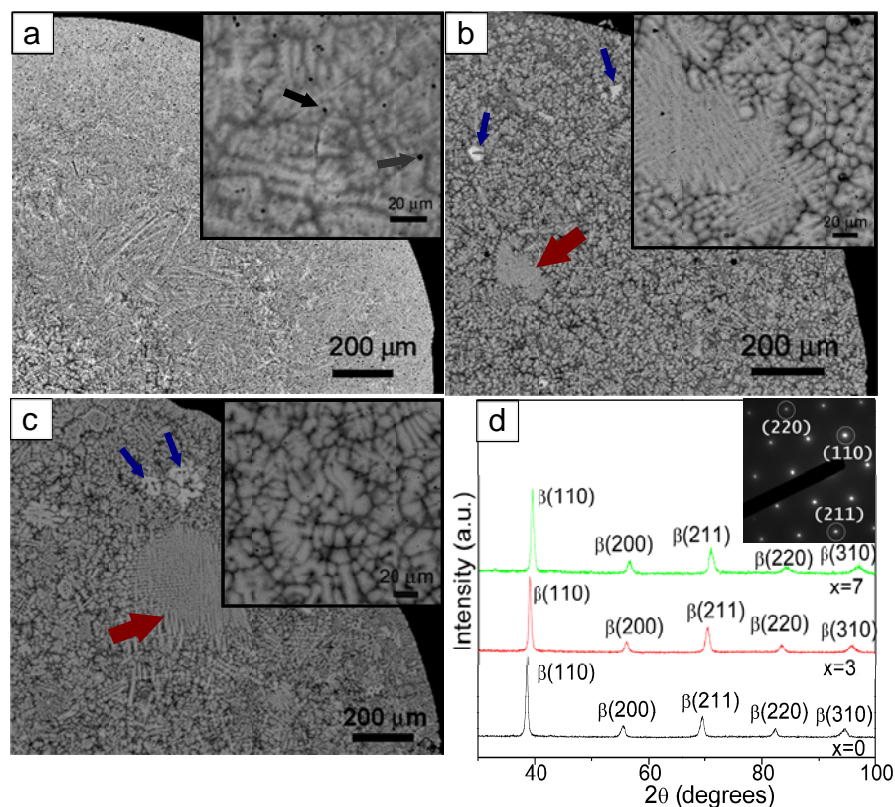


Fig. 1. SEM images (backscattered electrons) of the as-cast a) Ti-45Nb-7Zr-12.5Ta, b) Ti-45Nb-4Zr-12.5Ta-3Fe and c) Ti-45Nb-12.5Ta-7Fe rods. Upper insets: magnified images of the microstructure of the three compositions. d) XRD patterns obtained from the cross-section of the studied rods. Upper inset: SAED pattern of Ti-45Nb-12.5Ta-7Fe.

Table 1 summarizes the composition of the dark grey matrix and dendritic phases for the three samples along with the composition of the samples (in wt. %) according to EDX results. The relatively low atomic weight of Ti (47.867) and Fe (55.845), can explain the darker tonality of the matrix in all the alloys. Also few small (20-40 μm) particles (small blue arrows of Fig. 1b and c) are observed in the three alloys. The bright tonality of the particles can be attributed to their high content of Ta since the atomic weight of this element (i.e., 180.947 g/mol) is the highest amongst the elements present in these alloys.

Table 1. Overall composition for all the samples and of their dendritic and matrix phases in wt. %. Results obtained from EDX analysis.

Ti-45Nb-(7-x)Zr-12.5Ta-xFe	X = 0 wt. %	X = 3 wt. %	X = 7 wt. %
Average Composition	Ti ₃₆ Nb _{40.5} Zr _{12.8} Ta _{10.7}	Ti _{35.2} Nb _{45.1} Zr _{4.4} Fe _{2.7} Ta _{12.6}	Ti _{35.8} Nb _{45.9} Fe _{5.5} Ta _{12.8}
Dendritic phase	Ti _{35.5} Nb ₄₃ Zr ₉ Ta ₁₃	Ti ₂₈ Nb ₅₃ Zr ₃ Fe ₂ Ta ₁₄	Ti ₃₅ Nb ₄₆ Fe ₂ Ta ₁₇
Matrix	Ti ₄₃ Nb ₃₀ Zr ₂₂ Ta ₅	Ti ₄₅ Nb ₂₄ Zr ₁₄ Fe ₁₁ Ta ₆	Ti ₅₄ Nb ₃₄ Fe ₉ Ta ₃

It is noteworthy that, in spite of the composite-like microstructure of the investigated alloys, the XRD diffraction patterns of the three studied samples (Fig. 1d) only show high-intensity peaks associated to the β -Ti phase. The bright and dark areas in the SEM images are β -phase solid solutions containing different amounts of Ti, Fe, Zr, Nb and Ta. To confirm the presence of several elements in solid solution in the β -Ti phase, the Ti-45Nb-12.5Ta-7Fe sample was prepared for TEM. The imaged region consisted of β -phase rich in Ti and Fe but also contained Nb and Ta in solid solution (i.e., with composition Ti 54 %, Nb 34 %, Ta 3 wt. %, Fe 9

% all in wt. %). The formation of β -Ti could be expected considering that the elements composing the alloys are β -stabilizers (i.e., Fe, Nb and Ta) and/or neutral (i.e., Zr) [7]. For this reason, the XRD peaks are the result of the overlapping of several β -Ti solid solution phases. This may explain the slight variation of width and relative intensity of the peaks with the composition change. The calculated lattice parameter of the β -Ti solid solution phase for alloys with 3 and 7 wt. % Fe are 0.3278 and 0.3231 nm respectively, which are smaller than for pure β -Ti ($a = 0.3306$ nm) [8]. The decrease of lattice parameter with the progressive substitution of Zr by Fe is consistent with the atomic size of the two elements since the size of Fe (156 pm) is smaller than that of Ti (176 pm) and Zr (206 pm) [9]. This explains the tendency of the XRD peaks to become shifted towards higher angles with the increase in Fe content. This change in the lattice parameter has been confirmed by TEM. Indeed, the SAED pattern of the aforementioned region measured in the Ti-45Nb-12.5Ta-7Fe alloy (inset of Fig. 1d) reveals a shift in the atomic distances of (110), (211) and (220) planes, from the theoretical values (0.2337, 0.1349 and 0.1169 nm for pure β -Ti) to the measured ones (0.2272, 0.1327 and 0.1142 nm, respectively).

The mechanical properties of the alloys have been evaluated from nanoindentation tests with a maximum load of 500 mN load. This load is high enough to make indents that embrace all the phases during the test. Table 2 lists the values of hardness (H), reduced elastic modulus (E_r), plasticity index H/E_r and maximum indentation depth (h_{max}). The value E_r is normally smaller than the elastic modulus (E) since E_r takes into account the elastic strain that occurs in both the indenter tip and the sample [6]. The hardness and reduced Young's modulus decrease with the increase in Fe content, i.e., from $H = 3.181 \pm 0.09$ GPa and $E_r = 87.96 \pm 1.72$ GPa, in the Ti-45Nb-7Zr-12.5Ta alloy, to $H = 2.94$ GPa and $E_r = 75.39 \pm 1.92$ GPa in Ti-45Nb-12.5Ta-7Fe. These values are not far from those reported for other Ti-based alloys. The decrease of the reduced Young's modulus with the increase of Fe percentage can be explained from the cohesive energy values for Ti-Fe and Ti-Zr in the β -Ti phase. The cohesive energy of Ti-Fe can be calculated from the equation $0.5E_c^{Fe} + 0.5E_c^{Ti} - 0.22$ [10] where $E_c^{Fe} = 4.26$ eV/atom and $E_c^{Ti} = 4.85$ eV/atom are the cohesive energy of Fe and Ti, respectively. This leads to a cohesion energy for Ti-Fe of 4.34 eV/atom. This value is lower than the Ti-Zr cohesion energy (4.80 eV/atom) [11]. Hence, the bonding strength would be expected to be lower for Ti-Fe than for Ti-Zr, thus resulting in a decrease of Young's modulus when the Fe content increases. However, the addition of Fe appears to have little effect on the wear resistance. Indeed, the H/E_r parameter, which is indicative of the wear resistance [12,13], remains between 0.036 and 0.039 for the three investigated alloys. This value is very close to the H/E_r ratio measured in Ti-6Al-4V using the same indentation conditions [14]. This parameter is important since orthopaedic implants are expected to suffer from abrasion with bone and hard tissues leading to implant loosening and formation of wear debris that can result in inflammatory reactions [1]. Hence, it is important to develop new non-toxic compositions that preserve at least as good wear resistance as the commonly used Ti-6Al-4V.

Table 2. Hardness (H), reduced elastic modulus (E_r), plasticity index H/E_r and maximum indentation depth (h_{max}) for the maximum applied load of 500 mN.

Ti-45Nb-(7-x)Zr-12.5Ta-xFe	X = 0 wt.%	X = 3 wt.%	X = 7 wt.%
H (GPa)	3.181±0.090	3.000±0.015	2.940±0.134
E_r (GPa)	87.96±1.7	84.09±0.3	75.39±1.9
H/E_r	0.036	0.036	0.039
h_{max} (μ m)	2.87±0.05	2.91±0.006	3.07±0.08

Fig. 2 shows the potentiodynamic polarization curves of Ti-45Nb-(7-x)Zr-12.5Ta-xFe (x = 0, 3 and 7 wt. %) alloys in Hank's solution at 37°C. The corrosion potential, E_{corr} , for x = 3 is slightly more cathodic than in the Fe-free alloy (x = 0). However, when Zr is totally -replaced by Fe (x = 7) the E_{corr} shifts towards the anodic direction from -0.0127 V to -0.1917 V. Nevertheless,

not only the composition but also other factors such as the microstructure [15] and degree of alloying element segregation are expected to affect the E_{corr} .

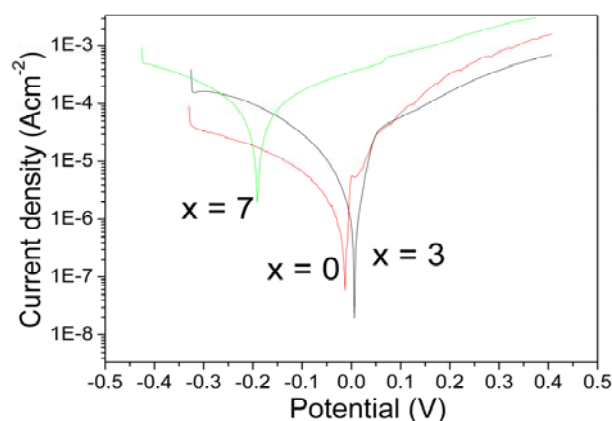


Fig. 2. Potentiodynamic polarization curves of the Ti-45Nb-(7-x)Zr-12.5Ta-xFe ($x = 0$, 3 and 7 wt. %) alloys in Hank's solution at 37°C.

The evolution of j_{corr} follows a more clear trend. The j_{corr} values increase from 1.469×10^{-6} A cm^{-2} to 2.148×10^{-5} A cm^{-2} when 3 wt. % Fe is added. Further addition up to 7 wt. % increases j_{corr} to 1.019×10^{-4} A cm^{-2} . These results are consistent with those reported for alloys belonging to the Ti-Fe system [16] where j_{corr} increases with the increase in Fe content. In particular, the E_{corr} value of pure Ti shifts anodically for small additions of Fe whilst larger percentages are shown to worsen the corrosion resistance [16]. This behaviour might be attributed to the formation of a Ti-Fe phase that destroys the passive TiO_2 surface film. Interestingly, although alloys of the Ti-Al-Fe system were reported to exhibit pitting corrosion [16], no breakdown potential was observed in our alloys, suggesting that none of these compositions have localized corrosion. Moreover, while the cathodic region of the Ti-45Nb-7Zr-12.5Ta alloy shows an anodic current peak at about 0.0069 V (see arrow in Fig. 2), no current peaks are observed for the Fe-containing alloys. The cathodic branch of the curves become also less noisy with the addition of Fe, suggesting that it increases the homogeneity of the corrosion layer.

To confirm the lack of pitting corrosion, the surfaces of Ti-45Nb-7Zr-12.5Ta and Ti-45Nb-12.5Ta-7Fe alloys after potentiodynamic polarisation in Hank's solution have been studied by SEM. Figs. 3 a and b correspond to the secondary and backscattered SEM images of Ti-45Nb-7Zr-12.5Ta alloy, respectively. Figs. 3 c and d correspond to the secondary and backscattered SEM image of Ti-45Nb-12.5Ta-7Fe alloy, respectively. The surfaces of both compositions are very similar and are mainly composed of scattered residues deposited from the Hank's solution.

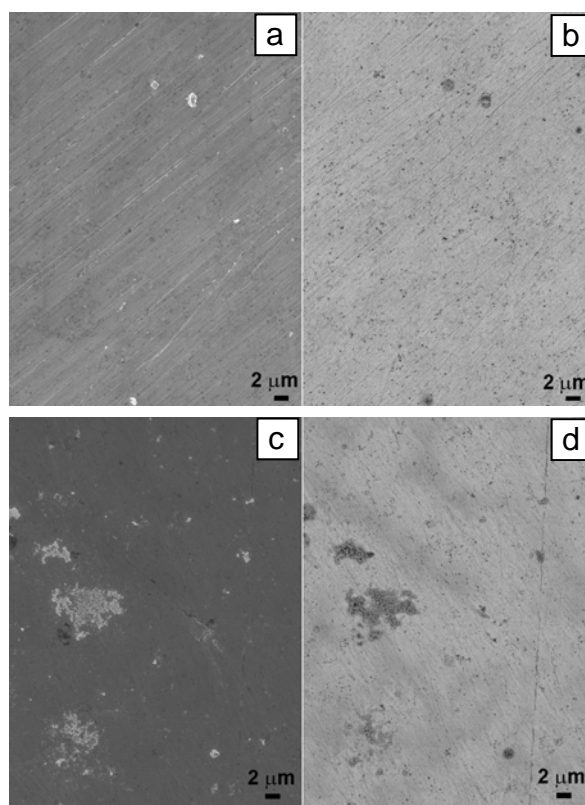


Fig. 3. SEM images of (a, b) Ti-45Nb-7Zr-12.5Ta and (c, d) Ti-45Nb-12.5Ta-7Fe alloy surfaces after potentiodynamic polarization in Hank's solution. Panels (a) and (c) correspond to secondary electron images whereas (c) and (d) are backscattered electron images.

In summary, new β -TNZT alloys with relatively low reduced Young's modulus and hardness have been obtained. Partial substitution of Zr by the more biocompatible and cheaper Fe element results in a slight decrease of the Young's modulus without worsening the corrosion behaviour. Moreover, the addition of Fe does not cause pitting corrosion which typically limits the applicability of biomaterials due to the wear debris originated from the breakdown of the protective passive layer. These alloys have thus potential interest to be used as biomaterials.

Acknowledgements

This work has been partially financed by the 2009-SGR-1292, MAT2011-27380-C02-01 and BioTiNet FP7-PEOPLE-2010-ITN-264635 research projects. S.G. is indebted to MICINN for the contract within the Juan de la Cierva Program. We acknowledge the SM for technical support. M.D.B. was partially supported by an ICREA Academia award.

References

- [1] M. Geetha, A.K. Singh, R. Asokamani, A.K. Gogia, *Prog. Mater. Sci.* **54**, 397 (2009).
- [2] J.A. Davidson, A.K. Mishra, P. Kovacs, R.A. Poggie, *Bio-Med. Mater. Eng.* **4**, 231 (1994).
- [3] S. Nag, R. Banerjee, H.L. Fraser, *Mater. Sci. Eng. C* **25**, 357 (2005).
- [4] R. Banerjee, S. Nag, J. Stechschulte, H.L. Fraser, *Biomaterials* **25**, 3413 (2004).
- [5] W.Y. Guo, J. Sun, J.S. Wu, *Materials Chemistry and Physics* **113**, 816 (2009).
- [6] W.C. Oliver, G.M. Pharr, *J. Mater. Res.* **7**, 1564 (1992).
- [7] M. Long, H.J. Rack, *Biomaterials* **19**, 1621 (1998).

- [8] H.Y. Kim, Y. Ikehara, J.I. Kim, H. Hosoda, S. Miyazaki, *Acta Mater.* **54**, 2419 (2006).
- [9] <http://www.webelements.com>
- [10] I. Sa, B.J. Lee, *Scripta Mater.* **59**, 595 (2008).
- [11] M. Abdel-Hady, H. Fuwa, K. Hinoshita, H. Kimura, Y. Shinzato, *Scripta. Mater.* **57**, 1000 (2007).
- [12] J. Halling, *Tribologia* **1**, 15 (1982).
- [13] J. Fornell, S. González, E. Rossinyol, S. Surinach, M.D. Baró, D.V. Louzguine-Luzgin, J.H. Perepezko, J. Sort, A. Inoue, *Acta Mater.* **58**, **6256** (2010).
- [14] J. Fornell, N. Van Steenberge, A. Varea, E. Rossinyol, E. Pellicer, S. Suriñach, M.D. Baró, J. Sort, *J. Mech. Behav. Biomed. Mater.* **6**, 53 (2012).
- [15] M. Geetha, U.K. Mudali, A.K. Gogia, R. Asokamani, B. Raj, *Corros. Sci.* **46**, 877 (2004).
- [16] N.V. Pimenova, T.L. Starr, *Electrochim. Acta* **51**, 2042 (2006).